Photo-induced electric responses in heterostructure of indium tin oxide/$(Bi_{1-x}Ca_x)FeO_{3-\delta}$/Au

Authors: C.- M. Hung, C.- S. Tu, Z.- R. Xu, V. Hugo Schmidt, and R. R. Chien

C.-M. Hung, C.-S. Tu, Z.-R. Xu, V.H. Schmidt, and R.R. Chien, "Photo-induced electric responses in heterostructure of indium tin oxide/(Bi 1-x Ca x FeO 3-δ /Au," IEEE Transactions on Magnetics 50, 1001804 (2014). doi: 10.1109/TMAG.2014.2327663.

Photo-Induced Electric Responses in Heterostructure of Indium Tin Oxide/$(Bi_{1-x}Ca_x)FeO_{3-\delta}$/Au

Cheng-Ming Hung[1], Chi-Shun Tu[1], Zhe-Rui Xu[2], V. Hugo Schmidt[3], and R. R. Chien[3]

[1]Graduate Institute of Applied Science and Engineering, Fu Jen Catholic University, New Taipei City 24205, Taiwan
[2]Department of Physics, Fu Jen Catholic University, New Taipei City 24205, Taiwan
[3]Department of Physics, Montana State University, Bozeman, MT 59717 USA

Photovoltaic effects in heterostructure of indium tin oxide (ITO)/$(Bi_{1-x}Ca_x)FeO_{3-\delta}$ multiferroic ceramics/Au ($x = 0.0$ and 0.15) have been measured under illuminations of $\lambda = 405$ and 445 nm. Open-circuit voltage (V_{oc}), short-circuit current density (J_{sc}), and power conversion efficiency (η) show strong dependences on light wavelength and intensity. For $\lambda = 405$ nm, V_{oc} and J_{sc} can reach 0.62 V and 0.042 A/m^2 for $BiFeO_3$ (BFO), and 0.48 V and 0.30 A/m^2 for $(Bi_{0.85}Ca_{0.15})FeO_{2.925}$ (BFO-15%Ca) at $I \sim 9.1 \times 10^2$ W/m^2. The maximum power conversion efficiency for $\lambda = 405$ nm can reach $\eta \sim 0.002\%$ for BFO and $\eta \sim 0.0035\%$ for BFO-15%Ca, which are comparable with 0.0025% observed in graphene/polycrystalline BFO/Pt films. A model based on forward p–n junction, reverse p–n junction and photo-excited currents in the interface between ITO film and $(Bi_{1-x}Ca_x)FeO_{3-\delta}$ ceramic, was developed to describe V_{oc} and J_{sc} as a function of incident light intensity. The theoretical fits agree well with experimental results. The depletion-region widths for $\lambda = 405$ nm were calculated as a function of light intensity. The calculated depletion-region widths without illumination are $d_o \sim 210$ nm in BFO and $d_o \sim 340$ nm in BFO-15%Ca.

***Index Terms*—$(Bi_{1-x}Ca_x)FeO_{3-\delta}$ ceramics, p-n junction model, photovoltaic (PV) effects, power conversion efficiency.**

I. Introduction

PEROVSKITE oxides, such as La-doped $Pb(Zr_xTi_{1-x})O_3$ [1]–[3], have shown photovoltaic (PV) responses. The PV effects of ferroelectric films depend on interface and dielectric permittivity of electrodes [2]. Theoretical analysis suggests that power-conversion efficiencies (η) in ferroelectric materials are in the range 10^{-4}%–10^{-2}% due to the short lifetime of photo-induced carriers [4]. The $(La_{0.7}Sr_{0.3})MnO_3/(Pb_{0.97}La_{0.03})(Zr_{0.52}Ti_{0.48})O_3$/Nb-$SrTiO_3$ films showed $\eta \sim 0.28\%$ under UV light at intensity (I) ~ 0.6 W/m^2 [3].

Multiferroic $BiFeO_3$ (BFO) possesses a G-type antiferromagnetic order with a spatially modulated spin structure [5]. Recent studies of multiferroic BFO have shown PV effects and photoconductivity with potential for applications [6]–[18]. The maximum power-conversion efficiencies (η) in Au/polycrystalline BFO/Pt [10], indium tin oxide (ITO)/polycrystalline BFO/Pt films [10], and graphene/polycrystalline BFO/Pt films [11] are, respectively, 0.005%, 0.125% at $I \sim 4.5$ W/m^2 and 0.0025% at $I \sim 10^3$ W/m^2.

The PV mechanisms of ferroelectric and multiferroic materials have not been well understood. Various PV mechanisms have been proposed for BFO films and single crystals, including asymmetric ferroelectric PV effect [1], [12], domain-wall model [13], and p-n junction model [18]. The recent first-principle calculation demonstrated that shift current is the dominant mechanism of the bulk PV effects in $BaTiO_3$ [19]. BFO and ITO films have shown p- and n-type semiconduction with carrier densities of $n_p \sim 10^{23}$ and $n_n \sim 10^{26}$–10^{27} m^{-3}, respectively [18], [20], [21]. The recent PV studies in the ITO/BFO ceramic/Au structure showed dependences on BFO thickness and illumination wavelength [22]. The photo-induced electricity can be attributed to photo-excited carriers in the depletion region between BFO ceramic and ITO film [22]. The electric properties of $(Bi_{1-x}Ca_x)FeO_{3-\delta}$ ceramics are sensitive to the oxygen pressure during synthesis and the conductivity can change from p-type semiconduction to a high level of ion conduction [23]. A p-n junction could be formed in Ca-doped BFO films by oxygen vacancy movement under an electric field [24].

Manuscript received February 26, 2014; revised May 23, 2014; accepted May 28, 2014. Date of current version November 18, 2014. Corresponding author: C.-S. Tu (e-mail: 039611@mail.fju.edu.tw).

Color versions of one or more of the figures in this paper are available online at http://ieeexplore.ieee.org.

II. Experimental Procedure

The BFO and $(Bi_{0.85}Ca_{0.15})FeO_{2.925}$ (BFO-15%Ca) ceramics were prepared by the solid-state reaction, in which Bi_2O_3, CaO, and Fe_2O_3 powders (purity $\geq$ 99.0%) were weighed in 1:0:1 and 0.85:0.3:1 ratios. The powders were mixed in an agate mortar with alcohol as a medium for more than 24 h. The chemical reactions are $Bi_2O_3 + Fe_2O_3 \rightarrow 2BiFeO_3$ and $0.85Bi_2O_3 + 0.3CaO + Fe_2O_3 \rightarrow 2(Bi_{0.85}Ca_{0.15})FeO_{2.925}$. The dried mixture was calcined at 800 °C for 3 h and was then pressed into a disk for sintering at 830 °C (10 h) for BFO and 925 °C (3 h) for BFO-15%Ca. Au and ITO films (~500 nm) were deposited on samples by the dc sputtering. The thickness of samples is $t = 0.2$ mm. Two diode continuous-wave lasers of $\lambda = 405$ and 445 nm were used for PV measurements. The laser beam was incident perpendicular to the surface with ITO film. For power-conversion efficiency (η), an adjustable load resistance was used to obtain the relation of current and voltage of the load, as shown in Fig. 1.

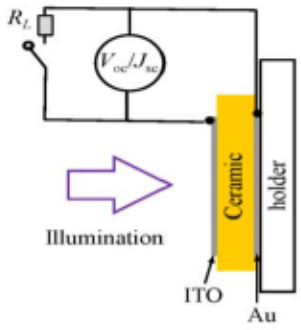

Fig. 1. Experimental configuration of PV effects.

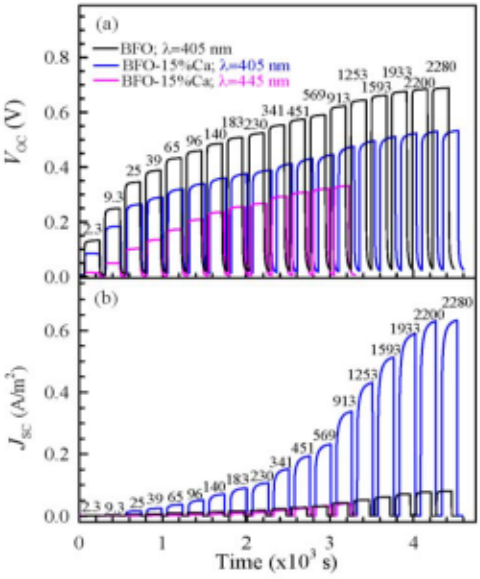

Fig. 2. (a) V_{oc} and (b) J_{sc} with increasing light intensity labeled on tops of peaks in unit of W/m^2.

III. Results And Discussion

Fig. 2 shows the open-circuit voltage (V_{oc}) and short-circuit current density (J_{sc}) as the laser was switched on and off. The illuminated V_{oc} and $J_{sc}$are plotted in Fig. 3. The illumination of $\lambda = 405$ nm ($E_{ph} \sim 3.06$ eV) induces stronger PV responses compared with $\lambda = 445$ nm ($E_{ph} \sim 2.78$ eV). The weaker PV responses under $\lambda = 445$ nm is due to smaller photon energy. The optical bandgap of BFO film is $E_{ph} \sim 2.74$ eV [7], [17]. For $\lambda = 405$ nm, V_{oc} and J_{sc} can reach 0.62 V and 0.042 A/m^2 for BFO, and 0.48 V and 0.30 A/m^2 for BFO-15%Ca at $I \sim 9.1 \times 10^2$ W/m^2. These values are comparable with $V_{oc} \sim 0.44$ V and $J_{sc} \sim 0.25$ A/m^2 at $I \sim 1 \times 10^3$ W/m^2 reported in graphene/polycrystalline BFO/Pt films [11].

To understand the illuminated V_{oc} and J_{sc}, we consider a heterojunction consisting of an n-type ITO film and a p-type BFO ceramic. The open-circuit voltage step across this p-n junction is assumed to be $-U_o$ without illumination. Under illumination, electron-hole pairs will be generated and decrease the depletion-region width. The decreased depletion-region width will lower the retarding voltage step

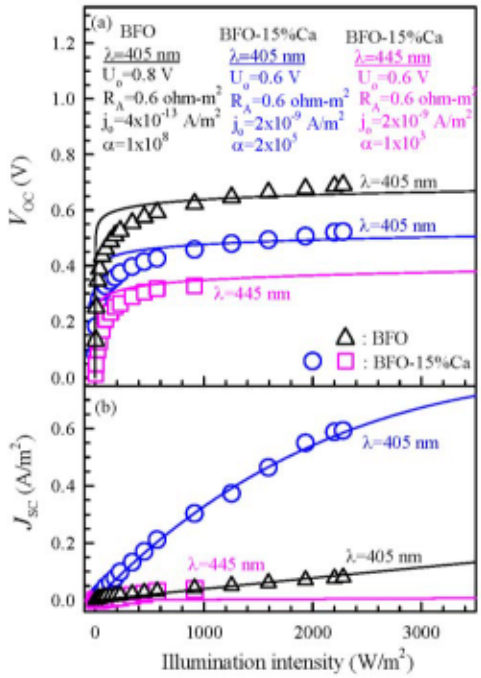

Fig. 3. (a) V_{oc} and (b) J_{sc}. The solid lines are the theoretical fits with parameters given in (a).

and correspondingly change the $-U_o$ voltage step to $-U(I)$. The measured open-circuit voltage V_{oc} can be described by

$$V_{oc}(I) = U_o - U_{oc}(I). \tag{1}$$

The total current density J includes three contributions. Two come from considering the junction as a diode that has forward and reverse current contributions [25]. The forward current is independent of illumination, but the reverse current depends on the decrease in the depletion-region width caused by illumination. The third contribution comes from the photo-excitation.

The first contribution is the forward p-n junction current density j_f from minority carriers that flow across the junction without hindrance because the field favors their flow. We call it forward current because it has the same sign as the photocurrent, but diode literature calls it reverse current. This forward current has hole and electron contributions

$$j_f = qD_p p_n/L_p + qD_n N_p/L_n \equiv j_o \tag{2}$$

where q is the hole charge, D_p is the hole diffusion constant, P_n is the carrier concentration of holes in the n-type region, L_p is their diffusion length, and corresponding definitions apply to D_n, N_p, and L_n. Here, j_o is the well-known diode saturation current density.

The second contribution to J is the reverse p-n junction current density j_r from majority carriers near the depletion region that have enough thermal energy to jump across the voltage barrier. From the standard model [25] for p-n diodes, and noting that these hole and electron contributions are negative, we have

$$j_r = -j_o \exp[q(U_o - U)/kT]. \tag{3}$$

The sum $-(j_f + j_r)$ from (2) and (3) is the well-known diode voltage-current characteristic expressed in our notation, and vanishes as it should for no illumination because then $U = U_o$.

The third contribution is the photo-excited current density j_p. The light intensity is assumed to decay mainly in the BFO-side depletion region (the energy gap in the ITO exceeds the photon energy) with a general form of $I(z) = I\exp(-z/\beta)$, where β is the attenuation length for which $\beta \ll d_p$. Thus, the absorbed intensity I_a in the depletion region can be estimated by $I_a = Id_p/\beta$. The creation rate of electron-hole pairs is estimated to be $I_a/(hc/\lambda)$. Then, j_p is given by

$$j_p = qd_pI\lambda/(hc\beta) \tag{4}$$

In the ITO-side depletion region ($-d_n < x < 0$), the net charge density $\rho_n = qn_n$ comes from the ionized donors, which have donated electrons to the conduction band. Similarly, in the depletion region ($0 < x < d_p$) of BFO side, $\rho_p = qn_p$ comes from the acceptors, which have accepted electrons from the valence band. Using 1-D Gauss' Law in the region $-d_n < x < 0$, the position-dependent E field is

$$E(x) = \int_{-d_n}^{x} (\rho_n/\varepsilon_o\varepsilon_n)dx' = (\rho/\varepsilon_o\varepsilon_n)(x + d_n) \tag{5}$$

Then, the total contribution from the n-type ITO and p-type BFO sides to $-U$ is

$$-U = (-q/2\varepsilon_o)(n_pd_p^2/\varepsilon_p + n_nd_n^2/\varepsilon_n) \tag{6}$$

where ε_o is the vacuum permittivity and ε_p and ε_n are the dielectric permittivities of ceramics and ITO film. The requirement that there is no net charge in the depletion region, gives $d_n = (n_p/n_n)d_p$. The carrier density $n_n \sim 10^{26}$–10^{27} m^{-3} of the n-type ITO film is much larger than $n_p \sim 10^{23}$ m^{-3} of the p-type BFO film [18]. Therefore, d_n in the ITO side is much less than d_p in the ceramic side. d_p can be designated as simply d. Then, (3) yields

$$\begin{aligned} -U &= -(qd^2n_p/2\varepsilon_o\varepsilon_p)(1 + n_p\varepsilon_p/\varepsilon_nn_n) = -Bd^2 \\ B &= (qn_p/2\varepsilon_o\varepsilon_p)(1 + n_p\varepsilon_p/\varepsilon_nn_n). \end{aligned} \tag{7}$$

For the open-circuit case ($J = 0$), we use $V_{oc} = U_o - U_{oc}$ and set $D_{oc} = d/d_o$, $\alpha = qd_o\lambda/(hc\beta j_o)$, $C = qBd_o^2/kT = qU_o/kT$, and T = 300 K. For no illumination, we have $j_f + j_r = 0$ and $d = d_o$, so for the open-circuit case we can use (1) to rewrite (3) as

$$j_r = -j_o\exp(qV_{oc}/kT). \tag{8}$$

Then, the intensity-dependent $D_{oc} = d_{oc}/d_o$ can be obtained from

$$J = j_f + j_p + j_r = j_o + j_oD_{oc}\alpha I - j_o\exp(qV_{oc}/kT) = 0. \tag{9}$$

Next, the V_{oc} can be obtained using (1) and (7)

$$V_{oc} = U_o - BD_{oc}^2d_o^2 = U_o(1 - D_{oc}^2). \tag{10}$$

For the short-circuit case (V = 0), the emf driving J_{sc} through an areaspecific resistance R_A is $U_o - U_{sc}$. Then, J_{sc} can be described by

$$J_{sc} = (U_o - U_{sc})/R_A = U_o(1 - D_{sc}^2/R_A). \tag{11}$$

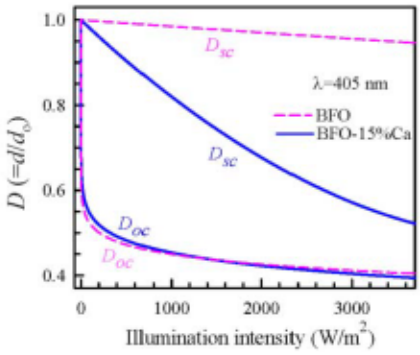

Fig. 4. D_{oc} ($= d_{oc}/d_o$) and D_{sc} ($= d_{sc}/d_o$) versus intensity for $\lambda = 405$ nm.

Here, $R_A = RS$ and $R = R_s + R_l$. R_s and R_l are the source and load resistances. S is the illuminated area. From modification of (9) and $U_o - U_{sc} = U_o(1 - D_{sc}^2)$, we have

$$J_{sc} = j_o\{1 + D_{sc}\alpha I - \exp[C(1 - D_{sc}^2)]\} \tag{12}$$

We subtract (11) from (12) and use $F = U_o/R_Aj_o$. Then

$$1 + D_{sc}\alpha I - \exp[C(1 - D_{sc}^2)] - F(1 - D_{sc}^2) = 0. \tag{13}$$

The intensity-dependent J_{sc} and $D_{sc}(= d_{sc}/d_o)$ can be obtained from (12) and (13).

The solid lines in Fig. 3 are fits of V_{oc} and J_{sc} for $\lambda = 405$ and 445 nm using (9)–(13) with parameters in Fig. 3(a). The experimental results and theoretical fits agree well with reasonable physical parameters. j_o may appear small but it does allow for a reverse current, which significantly reduces the short-circuit current density, and minimizing such reduction is a consideration for p-n junction devices.

The dielectric permittivities of BFO and BFO-15%Ca ceramics at room temperature are $\varepsilon_p \sim 50$ [26] and $\varepsilon_p \sim 170$ for measuring frequency $f = 1$ MHz. Assume that the carrier densities of BFO and BFO-15%Ca are similar to $n_p \sim 10^{23}$ m^{-3} of the p-type BFO film [18]. From (7), $d_o \sim (2\varepsilon_o\varepsilon_pU_o/qn_p)^{1/2}$, the unilluminated depletion-region widths are $d_o \sim 210$ nm in BFO and $d_o \sim 340$ nm in BFO-15%Ca, which are consistent with the depletion layer (a few hundred nanometers) between ITO and BFO films [18]. Based on fitted parameters in Fig. 3(a), the optical attenuation length ($\beta = qd_o\lambda/hc\alpha j_o$) is ~ 2.0 mm for $\lambda = 405$ nm in BFO. The β values in BFO-15%Ca are ~ 0.3 mm for $\lambda = 405$ nm and ~ 6 cm for $\lambda = 445$ nm. The calculated β values consider only for absorption caused by electron-hole creation, and are much larger than actual values, because of other absorptions and dissipation mechanisms, such as internal reflection by grain boundaries and charge recombination. These factors may cause fitting deviations in V_{oc} at low illumination, as observed in Fig. 3(a).

Fig. 4 shows the ratios of depletion-region widths of $D_{oc}(= d_{oc}/d_o)$ and $D_{sc}(= d_{sc}/d_o)$ as a function of illumination intensity. The D_{oc} is more sensitive and decreases roughly exponentially with light intensity because V_{oc} increases almost to U_o. D_{sc} declines only slightly in BFO with light intensity because $i_{sc}R_A \ll U_o$ even at the highest intensity. The rapid reduction of D_{oc} with light intensity, suggests that the charge recombination in the depletion region is more effectively in the

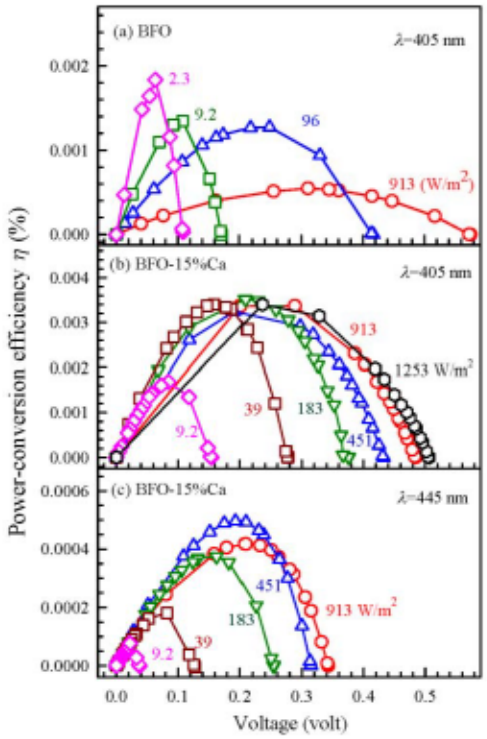

Fig. 5. Power conversion efficiency η versus measured voltage under illuminations of $\lambda = 405$ and 445 nm for various intensities.

open-circuit case ($J = 0$), because the photo-induced carriers cannot flow away from the junction to the external circuit, but must stay there and have much more probability to recombine.

The relations of power-conversion efficiency (η) versus voltage (V) for $\lambda = 405$ and 445 nm are shown in Fig. 5. The power-conversion efficiencies for $\lambda = 405$ nm are much larger than those for $\lambda = 445$ nm. The maximum η for $\lambda = 405$ are 0.002% for BFO and 0.0035% for BFO-15%Ca.

IV. Conclusion

The ITO/$(Bi_{1-x}Ca_x)FeO_{3-\delta}$ ceramic/Au heterostructure exhibits significant PV responses and power conversion under illumination of $\lambda = 405$ nm. The enhanced PV effects in BFO-15%Ca may associate with oxygen vacancy movement and $Fe^{3+} \rightarrow Fe^{4+}$ transformation due to the $Bi^{3+} \rightarrow Ca^{2+}$ substitution. The maximum power conversion efficiency for $\lambda = 405$ nm can reach $\eta \sim 0.002\%$ for BFO and $\eta \sim 0.0035\%$ for BFO-15%Ca. The model based on forward and p-n junction and photo-excited currents, can well describe the illuminated open-circuit voltage (V_{oc}), short-circuit current density (J_{sc}), and depletion-region width (d) as a function of light intensity. The potential steps across the depletion region for no illumination are $U_o \sim 0.8$ V in BFO and $U_o \sim 0.6$ V in BFO-15%Ca.

Acknowledgment

This work was supported by the National Science Council of Taiwan under Grant 100-2112-M-030-002-MY3.

References

[1] P. Poosanaas, A. Dogan, S. Thakoor, and K. Uchino, "Influence of sample thickness on the performance of photostrictive ceramics," *J. Appl. Phys.*, vol. 84, no. 3, pp. 1508–1512, Aug. 1998.

[2] M. Qin, K. Yao, and Y. C. Liang, "Photovoltaic mechanisms in ferroelectric thin films with the effects of the electrodes and interfaces," *Appl. Phys. Lett.*, vol. 95, no. 2, p. 022912, 2009.

[3] M. Qin, K. Yao, and Y. C. Liang, "High efficient photovoltaics in nanoscaled ferroelectric thin films," *Appl. Phys. Lett.* vol. 93, no. 12, p. 122904, 2008.

[4] V. M. Fridkin, "Bulk photovoltaic effect in noncentrosymmetric crystals," *Crystallogr. Rep.*, vol. 46, no. 4, pp. 654–658, 2001.

[5] I. Sosnowska, T. P. Neumaier, and E. Steichele, "Spiral magnetic ordering in bismuth ferrite," *J. Phys. C, Solid State Phys.*, vol. 15, no. 23, pp. 4835–4846, 1982.

[6] T. Choi, S. Lee, Y. J. Choi, V. Kiryukhin, and S.-W. Cheong, "Switchable ferroelectric diode and photovoltaic effect in $BiFeO_3$," *Science*, vol. 324, no. 5923, pp. 63–66, 2009.

[7] W. Ji, K. Yao, and Y. C. Liang, "Bulk photovoltaic effect at visible wavelength in epitaxial ferroelectric $BiFeO_3$ thin films," *Adv. Mater.*, vol. 22, no. 15, pp. 1763–1766, 2010.

[8] N. A. Spaldin, S.-W. Cheong, and R. Ramesh, "Multiferroics: Past, present, and future," *Phys. Today*, vol. 63, no. 10, p. 38, 2010.

[9] C. Himcinschi *et al.*, "Substrate influence on the optical and structural properties of pulsed laser deposited $BiFeO_3$ epitaxial films," *J. Appl. Phys.*, vol. 107, no. 12, pp. 123524-1–123524-5, Jun. 2010.

[10] B. Chen *et al.*, "Effect of top electrodes on photovoltaic properties of polycrystalline $BiFeO_3$ based thin film capacitors," *Nanotechnology*, vol. 22, no. 19, p. 195201, 2011.

[11] Y. Zang *et al.*, "Enhanced photovoltaic properties in graphene/polycrystalline $BiFeO_3$/Pt heterojunction structure," *Appl. Phys. Lett.*, vol. 99, no. 13, pp. 132904-1–132904-3, Sep. 2011.

[12] W. Ji, K. Yao, and Y. C. Liang, "Evidence of bulk photovoltaic effect and large tensor coefficient in ferroelectric $BiFeO_3$ thin films," *Phys. Rev. B*, vol. 84, p. 094115, Sep. 2011.

[13] S. Y. Yang *et al.*, "Above-bandgap voltages from ferroelectric photovoltaic devices," *Nature Nanotechnol.*, vol. 5, no. 2, pp. 143–147, 2010.

[14] H. T. Yi, T. Choi, S. G. Choi, Y. S. Oh, and S.-W. Cheong, "Mechanism of the switchable photovoltaic effect in ferroelectric $BiFeO_3$," *Adv. Mater.*, vol. 23, no. 30, pp. 3403–3407, 2011.

[15] Y. B. Chen *et al.*, "Ferroelectric domain structures of epitaxial (001) $BiFeO_3$ thin films," *Appl. Phys. Lett.*, vol. 90, no. 7, pp. 072907-1–072907-3, Feb. 2007.

[16] B. Kundys, M. Viret, D. Colson, and D. O. Kundys, "Light-induced size changes in $BiFeO_3$ crystals," *Nature Mater.*, vol. 9, pp. 803–805, Jul. 2010.

[17] J. F. Ihlefeld *et al.*, "Optical band gap of $BiFeO_3$ grown by molecular-beam epitaxy," *Appl. Phys. Lett.*, vol. 92, no. 14, p. 142908, 2008.

[18] S. Y. Yang *et al.*, "Photovoltaic effects in $BiFeO_3$," *Appl. Phys. Lett.*, vol. 95, no. 6, p. 062909, 2009.

[19] S. M. Young and A. M. Rappe, "First principles calculation of the shift current photovoltaic effect in ferroelectrics," *Phys. Rev. Lett.*, vol. 109, p. 116601, Sep. 2012.

[20] H. Kim *et al.*, "Electrical, optical, and structural properties of indium–tin–oxide thin films for organic light-emitting devices," *J. Appl. Phys.*, vol. 86, no. 11, p. 6451, 1999.

[21] M. Rottmann and K.-H. Heckner, "Electrical and structural properties of indium tin oxide films deposited by reactive DC sputtering," *J. Phys. D, Appl. Phys.*, vol. 28, no. 7, p. 1448, 1995.

[22] C. S. Tu, C. M. Hung, V. H. Schmidt, R. R. Chien, M. D. Jiang, and J. Anthoninappen, "The origin of photovoltaic responses in $BiFeO_3$ multiferroic ceramics," *J. Phys., Condens. Matter*, vol. 24, no. 49, p. 495902, 2012.

[23] N. Masó and A. R. West, "Electrical properties of Ca-doped $BiFeO_3$ ceramics: From p-type semiconduction to oxide-ion conduction," *Chem. Mater.*, vol. 24, no. 11, pp. 2127–2132, 2012.

[24] K. K. Bharathi *et al.*, "Detection of electrically formed photosensitive area in Ca-doped $BiFeO_3$ thin films," *Appl. Phys. Lett.*, vol. 102, no. 1, pp. 012908-1–012908-5, Jan. 2013.

[25] L. V. Azaroff and J. J. Brophy, *Electronic Processes in Materials*. New York, NY, USA: McGraw-Hill, 1963, ch. 10.

[26] C.-S. Tu, W.-C. Yang, V. H. Schmidt, and R. R. Chien, "Origins of dielectric response and conductivity in $(Bi_{1-x}Nd_x)FeO_3$ multiferroic ceramics," *J. Appl. Phys.*, vol. 110, no. 11, pp. 114114-1–114114-5, Dec. 2011.